Quantum modeling (DFT) and experimental investigation of beryllium–tungsten alloy formation



2009 J. Phys.: Condens. Matter 21 355011

(http://iopscience.iop.org/0953-8984/21/35/355011)

IOP Publishing Journal of Physics: Condensed Matter

J. Phys.: Condens. Matter **21** (2009) 355011 (9pp) doi:10.1088/0953-8984/21/35/355011

# Quantum modeling (DFT) and experimental investigation of beryllium–tungsten alloy formation

**A Allouche[1], A Wiltner[2] and Ch Linsmeier[2]**

[1] Physique des Interactions Ioniques et Moléculaires, CNRS and Université de Provence (UMR6633), Campus Scientifique de Saint Jérôme, service 242, 13397 Marseille Cedex 20, France

[2] Max-Planck-Institut für Plasmaphysik, EURATOM Association, Boltzmannstraße 2, 85748 Garching bei München, Germany

E-mail: alain.allouche@univ-provence.fr and linsmeier@ipp.mpg.de

Received 30 April 2009, in final form 16 July 2009
Published 11 August 2009
Online at stacks.iop.org/JPhysCM/21/355011

**Abstract**

Beryllium, tungsten and carbon are planned as wall-cladding materials for the future international tokamak ITER. Be and W will be the dominant components and therefore the formation of binary Be–W alloys under plasma action is one of the most important issues in plasma–wall interaction processes at the first wall. This paper proposes a first-principles density functional theory (DFT) study of beryllium atom retention in tungsten, and a discussion of the results in relation to the available experimental data. In a first step, the beryllium adsorption energy is calculated on the W(100) and W(111) surfaces. Further, the activation barrier for the surface–subsurface diffusion step and subsequent bulk diffusion steps are considered. For each calculation, the electronic structure of the formed compound is analyzed through projected density of states (DOS) calculations.

(Some figures in this article are in colour only in the electronic version)

## 1. Introduction

A tokamak [1] is a toroidal device where a deuterium–tritium (D–T) plasma is magnetically confined in order to reach an energy and concentration high enough to induce the thermonuclear fusion of the two nuclei, thus releasing a very large amount of energy:

$$\mathrm{D} + \mathrm{T} \rightarrow \mathrm{He}\ (3.5\ \mathrm{MeV}) + \mathrm{n}\ (14.1\ \mathrm{MeV}).$$

Nuclear fusion of light atoms is the fundamental process in the Sun, which provides energy to our solar system. ITER is an international research tokamak project, which is intended as an experimental feasibility confirmation of magnetic confinement for future power generation through thermonuclear fusion. The construction of ITER in Cadarache (France) started in 2007, and the first plasma ignition is expected in 2018 [2].

Although the inner wall of the tokamak chamber is isolated from the hot plasma by confinement in magnetic fields, the wall is still subjected to atomic or radical fragment fluxes coming from the boundary plasma, a much colder plasma. Therefore, the inner wall cladding of a tokamak is made up of materials of specific mechanical, magnetic, thermal and electric properties: the ITER's first wall will be constituted of beryllium, tungsten and carbon. During operation, the plasma particles will induce chemical erosion and physical sputtering processes. Due to transport of the impurity atoms and redeposition, beryllium films will be deposited on the tungsten parts, and inversely, contamination of the beryllium surfaces by tungsten is possible. As a consequence, parts of the first wall will no longer be composed of pure metals, but of alloys with altered chemical and physical properties.

Since the fundamental reaction processes in the Be–W system are very difficult, or impossible, to study *in situ* in a tokamak, dedicated experiments are developed on a laboratory scale, notably by the Doerner [3–5] and the Linsmeier [6–9] groups. These two series of experiments are different and complementary. In the PISCES-B experiments (Doerner's group), the Be–W alloy is observed after tungsten exposure

 

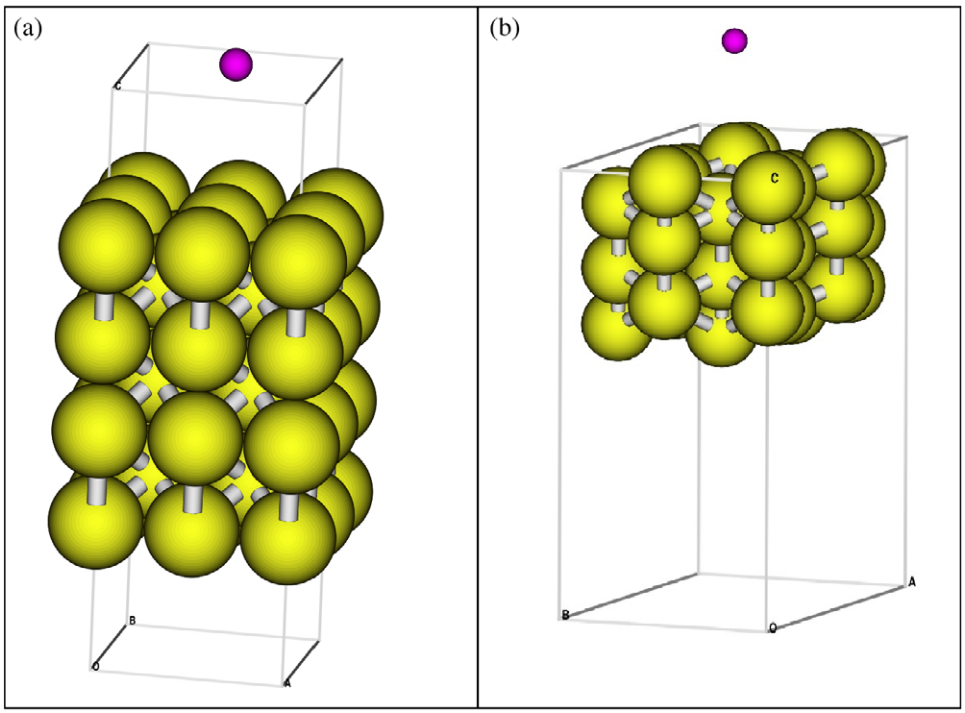


**Figure 1.** Periodic crystal working cells used to represent (a) the W(100) tungsten slab, (b) the W(111) tungsten slab.

to a beryllium-seeded deuterium plasma at high fluences, in which the Be–W mixed material is formed in out-of-thermal-equilibrium conditions. In the Linsmeier group's experiments, the goal is to study the potential reaction and diffusion processes of the two metals after heating a sample of one of them supporting a thin film of the other.

However, in both cases, the elementary steps underlying the alloy formation mechanisms can only be completely identified through theoretical contributions, and the quantum theory in the first-principles DFT formalism is the most reliable approach to determine the fundamental processes of the first steps of beryllium–tungsten mixed material formation. A first contribution dealt with tungsten adsorption on the beryllium (0001) surface [10] and the present paper makes use of the same general formalism to study the reverse system, i.e. adsorption of beryllium on tungsten. In the experiments so far, the simulation of tokamak reactions were performed on polycrystalline tungsten samples. For this first quantum approach we have selected two of the most stable tungsten surfaces, W(100) and W(111) [11]. The structures of these two surfaces are different enough to be representative of a polycrystalline tungsten film. The first one being simpler in its geometrical as well as its electronic structure, it deserves a more detailed analysis. From there, the interpretation will be extended to interpret the more complex behavior of W(111).

## 2. Quantum study

### *2.1. Computational details*

The calculations were performed within the framework of the spin-polarized gradient-corrected density functional theory. The exchange as well as the correlation functionals are Perdew–Burke–Ernzerhof (PBE). A plane-wave basis set was used with an energy cutoff of 32 Ryd (435 eV); the ionic core potential was modeled using Vanderbilt ultrasoft pseudopotentials. Integration in the first Brillouin zone was performed using the $6\times6\times1$ points Monkhorst–Pack sampling.

The stationary state structures were optimized using the quasi-Newton Broyden–Fletcher–Goldfarb–Shanno (BFGS) generalized algorithm. All the atoms were included in the optimization procedure, without any geometry or symmetry constraint. All the energy calculations were carried out using the *Quantum-Espresso* package[3]. The tungsten pseudopotential is taken from the package's library. We have carefully tested that it reproduces with a sufficient accuracy the cell parameter (3.186 Å, experimental: 3.165 Å), the cohesive energy (9.01 eV, experimental: 8.90 eV) [13] and the relaxation of the surfaces. As the results, our working systems are:

(i) W(100) crystal working cell is orthorhombic (cell parameters: 6.372 Å × 6.372 Å × 20 Å), it includes 29 tungsten atoms and 7 layers (figure 1(a)). This system proved to be a good compromise between calculation feasibility and accuracy. For example, the surface relaxation calculation yields −10.6% for the first interlayer relaxation, which is in good agreement with other work, −10.7% [11].

(ii) The W(111) crystal cell is hexagonal (9.013 Å × 9.013 Å × 20 Å), it includes 36 W and 9 layers (figure 1(b)). The first interlayer relaxation is larger than the W(100) one, 20%, also in good agreement with previous works [14].

[3] Quantum-ESPRESSO is a community project for high-quality quantum-simulation software, based on density functional theory, and coordinated by Paolo Giannozzi. See [12].

The beryllium pseudopotential is home calculated, it is described and tested in detail in [15].

The interaction of the beryllium atom with this slab is investigated through a potential energy surface (PES) that is determined in scanning the beryllium position from far above the surface to a point located inside the bulk at an equal distance from the two surfaces delimiting the slab. In practice far above the surface is 5 Å above the geometrical center of the slab, where the potential energy surface shows a flat curve (see figure 3 below). All the other coordinates are optimized without any restriction.

The interaction energy of $n$ W atoms with a beryllium slab is defined as (the same for $n$ Be on/in the W slab)

$$\Delta E = [E(\text{Be cell} + n\text{W}) - E(\text{Be cell}) - nE(\text{W})]/n. \quad (1)$$

### 2.2. Results from DFT calculations

*2.2.1. Interaction of a single beryllium atom with the W(100) surface.* The pseudo-valence tungsten atom electronic DOS (density of states) includes $(5s, 5p)^8(5d)^4(6s)^2$ electrons. From orbital frontier theory [16], it is well known that the orbital states of a metal directly involved in interaction with the adsorbate orbitals are the ones closest to the Fermi level. Of course the surfaces of transition metals also have open sp bands and therefore also form bonds to adsorbates, however it was shown [17] that the presence of d states enables a further bonding interaction between the metal d states and the adsorbate states, and this interaction is predominant for the understanding of the adsorption process. The DOS corresponding to the non-interacting system is displayed in figure 2(a). The Fermi energy ($E_F$) level crosses the W(5d) band, whereas the Be(2s) energy levels are right below $E_F$ and the Be(2p) are empty and degenerated. The calculated Löwdin atomic charges [18] corroborate this distribution since the total beryllium charge is 1.97 electron with 1.91 2s and 0.06 2p. On this figure also, it is worth noting that the density of states corresponding to the surface layer is quite different from that of inner layers: the surface induces an important shift of the larger peak towards the Fermi level. This phenomenon has been mentioned and discussed treating of the W(001) surface [19–21]. The peak at 1.6 eV is due to the W($d_{z^2}$) energy surface energy level, the peak located around −0.25 eV corresponds to the degenerated $d_{zx}$ and $d_{zy}$.

The beryllium atom adsorbs on the surface without a barrier in a −2.3 eV deep potential well (figure 3), 1.72 Å above the surface in a bridge position between two W atoms (figure 4), no other minimum has been found. The stability of this adsorption site is provided by combining the W(5d) and Be(2p) atomic wavefunctions (figure 2(b)). Globally, the beryllium atom total charge remains unchanged (1.90 electron), but with a large transfer from 2s to 2p. The Löwdin charges are 0.73 and 1.17 electron, respectively. The W–Be–W arrangement in figure 4 defines a plane parallel to $(yz)$. Figure 2(b) clearly shows that the $2p_z$ and $2p_x$ orbitals play a quite similar role and their contribution to the valence band is very diffuse. On the contrary, the $2p_y$ contribution is very localized above and below the Fermi level, its maximum coincides with the maximum of the surface layer DOS. At the same time, the surface peak in the conduction band is noticeably smaller, which signifies that the Be–W binding is ensured by an efficient combination of 5d orbitals ($d_{z^2}$ with contribution from the $d_{zx}$ and $d_{zy}$ components) of the superficial tungsten atoms and the beryllium $2p_y$ (figure 4). Within this analysis, it can therefore be considered that the beryllium atom adopts an $sp^2$-like hybridization scheme with a partially filled $\pi$-like orbital ($2p_y$) parallel to the surface plane and two hybrids in the $(zx)$ plane.

Note must be taken of a small shift (0.15 eV) towards the Fermi level of the superficial W(5d) energy levels involved into the binding with beryllium; then it can be expected that their combination with and an eventual binding with a second beryllium atom should be facilitated.

From the minimum in adsorption energy, the barrier which Be must overcome in order to penetrate into the subsurface position is about 3.6 eV (figure 3, difference between the potential well energy and the higher maximum in energy). But beyond this point, going deeper into the bulk seems much easier since the local minimum after the transition point is only 0.7 eV lower in energy respect to it. However, the system's total energy at this point of the PES does not induce an energy stabilization in comparison to the total energy of the two non-interacting systems (it is even about 1 eV higher), and much higher than the total energy of the adsorbed system.

The beryllium subsurface trapping is accompanied by an important gain in charge since 0.42 electron is transferred from the tungsten reservoir to the benefit of the Be(2p) orbitals, which now bear 1.95 electron equally distributed over the three components (figure 2(c)). In this trapping site, six tungsten neighbors surround the beryllium atom: two of them are located at a distance of 1.98 Å, two at 2.16 Å and the last pair at 2.40 Å. Comparing figures 2(b) and (c) it can be noted that the Be(2p) contribution to the total valence band is more concentrated around the Fermi level (the region of the most reactive orbitals) when Be is adsorbed, and much more diffuse between −10 and 0 eV when Be is embedded in the bulk. This must be related to the directional character of the 2p orbitals. Embedded in the W electron bath, Be loses its $2sp^2$-type preferred directions, the three components bear the same electronic charge, and since the total net charge is negative (−0.42 electrons) the Fermi repulsion between this electron density and the metal electron bath destabilizes the system.

*2.2.2. Interaction of a single beryllium atom with the W(111) surface.* The geometry and symmetry of the W(100) surface are simpler than those of W(111), and therefore easier to interpret, but qualitatively the two systems are similar. However, the W(111) surface undergoes a larger relaxation than the W(100): the two first interlayer distances are contracted by −20% and −16%, whereas the third one is dilated by +12%. The multilayer relaxation geometry of the W(111) surface depends strongly on the method and the number of layers used, nevertheless most of the calculations predict the same relaxation pattern, of a triplet of W layers moving towards each other and an expansion of the next layer spacing [14]. Our results are in good general agreement with the other quantum calculations [17, 13, 22].

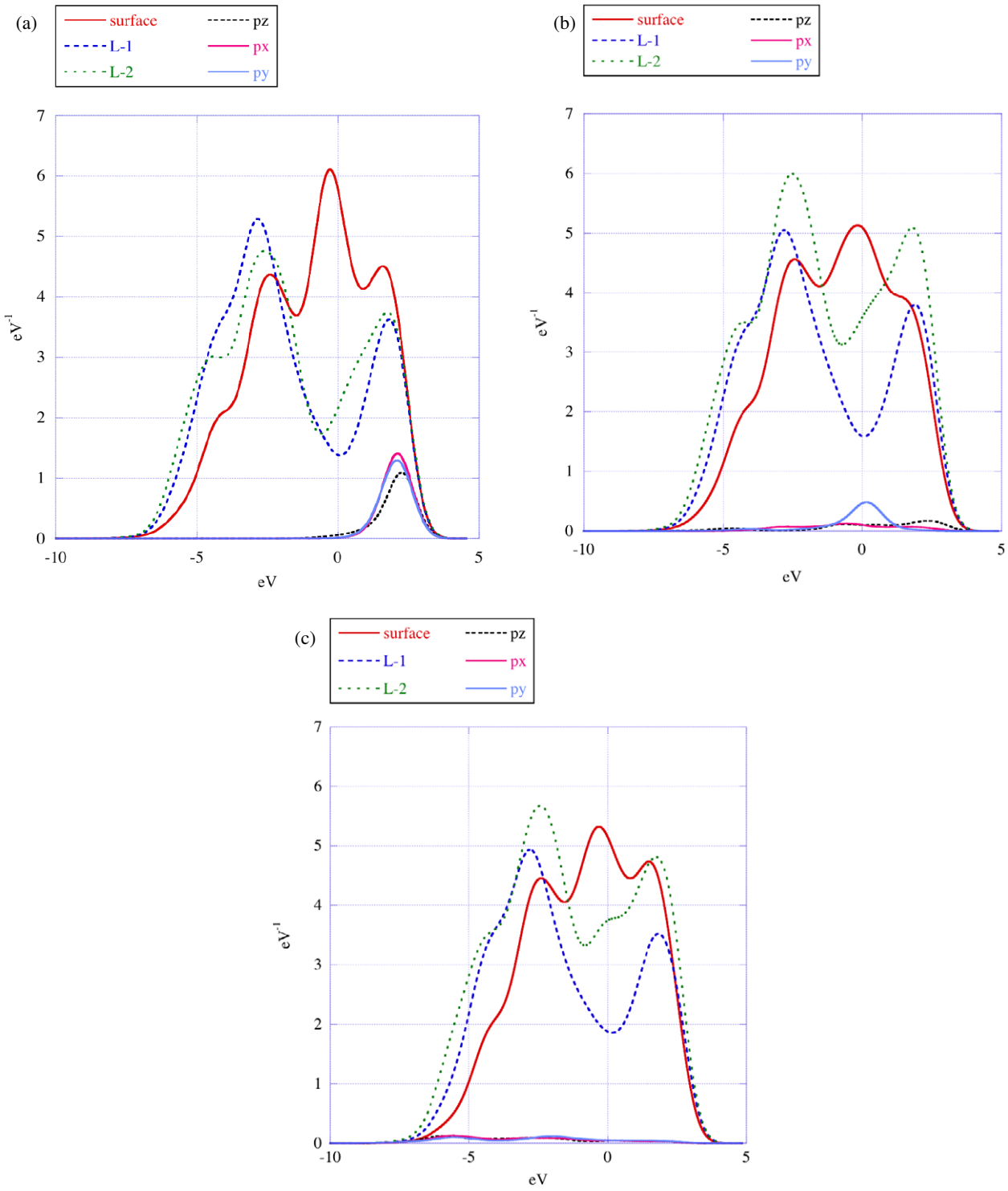


**Figure 2.** (a) Electronic density of states for the non-interacting Be–W(100) system presented in figure 1, the beryllium atom is located in the cell vacuum, 5 Å above the surface. The origin of energies is fixed at the Fermi level, only the W(5d) of the three upper layers of the tungsten slab and the three Be(2p) components DOSs are presented, signaled as $p_x$, $p_y$ and $p_z$ (same conventions in the next figures), $L_{-1}$ indicates the first layer below the surface, $L_{-2}$ the second layer and so forth. (b) System DOS perturbation (compared to (a)) induced by Be adsorption. (c) System DOS perturbation induced by Be trapping into the bulk.

The consequence for our system is that the three first upper layers (denoted as the surface layer S, $L_{-1}$, $L_{-2}$, ...) are closer to another than layers in the bulk. In difference to the W(100) case [23], the S, $L_{-1}$ and $L_{-2}$ DOSs projected on the W(d) orbitals (figure 5) look quite similar. However, compared to the non-interacting system, a shift towards lower energies is observed at the maximum in the valence band; this shift is small from the three upper layers, but becomes notably larger for the $L_{-3}$ layer. Therefore, the slab relaxation for the W(111) system induces an effect qualitatively similar to that observed

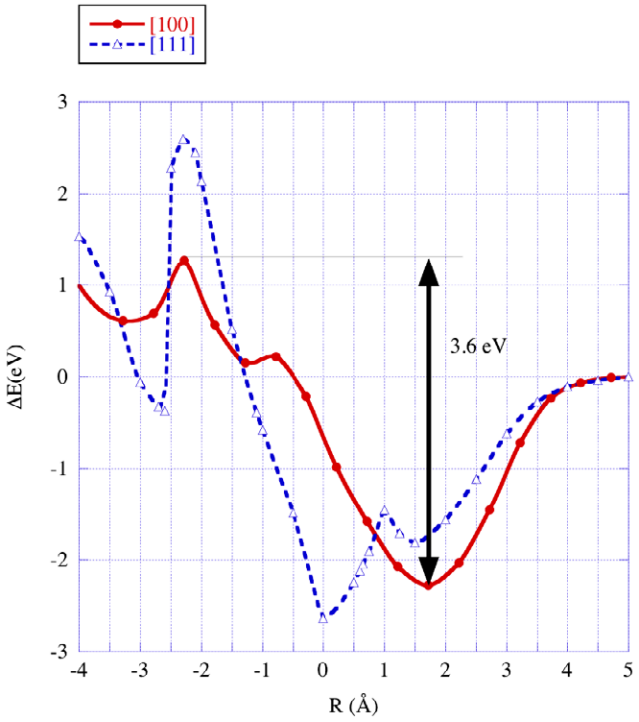


**Figure 3.** Energy profiles associated to one beryllium atom approaching the W(100) (continuous line) and W(111) (broken line) slabs. $R$ is the distance from the beryllium atom to the tungsten surface (point 0 on the $R$ axis). The energies $\Delta E$ are referred to the respective non-interacting system (at $R = 5$ Å). The first energy minima on the right side correspond to adsorption. The maxima on the left side correspond to the barrier to Be inclusion into the host metal.

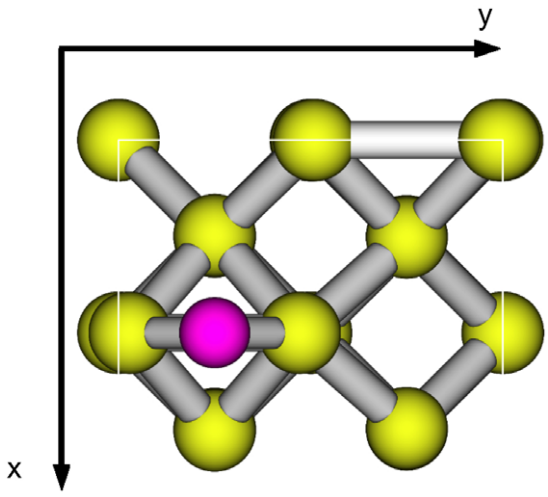


**Figure 4.** Beryllium atom adsorption site on the W(100) surface.

on the W(100) system [23]: the beryllium–tungsten interaction will be more efficient on or near the surface than within the bulk. These considerations, and also the contraction of the three upper layers that increases the electron density near the surface [17], imply that the respective action of each of these 'superficial layers' towards the beryllium will be cumulative and the resulting reactivity towards Be enhanced in the positive as well as in the negative direction: the minima in energy,

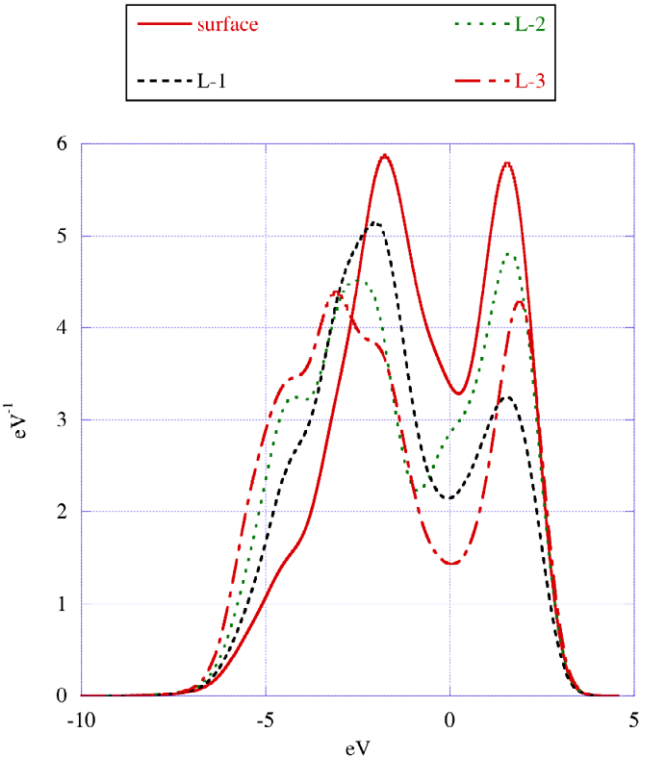


**Figure 5.** W(5d) projected electronic density of states for the non-interacting W(111) system, same conventions as in figure 2(a), the Be(2p) projected DOS are not represented.

as well as the barriers of activation, are larger along the Be trajectory compared to the former W(100) case.

The energy profile presented in figure 3 reflects this electronic structure. The adsorption well is split into two minima; a first minimum (−1.8 eV) is found when the beryllium atom is 1.5 Å above the tungsten surface. A small barrier (0.4 eV) corresponds to the crossing of the surface layer and the reorganization of the surface around the arriving beryllium, this barrier was not observed in the former case. Another deeper minimum (−2.6 eV) occurs when the beryllium atom is embedded into the surface plane above the $L_{-1}$ layer, it corresponds to the adsorption minimum in the W(100) case. The minimum splitting is due to the W(111) relaxation which narrows the first interlayer distance, therefore the surface and $L_{-1}$ electronic densities are very close to each other, and one minimum occurs above the surface and the second one (deeper) when Be is slightly embedded into the surface layer.

For the same structural reason as above, the barrier necessary to overcome in order to cross the $L_{-1}$ and $L_{-2}$ layers is much larger than in the W(100) case: 5.2 eV. But again the energy minimum corresponding to the beryllium trapping into the bulk brings no noticeable stabilization of the system, since it is only located 0.4 eV below the non-interacting system energy. It must therefore be considered that the inclusion of a beryllium atom into the W(111) slab is not an energetically favorable configuration.

*2.2.3. Multiple adsorptions on the W(111) surface and adlayer structure.* The analysis of the modifications to the projected

DOS of the tungsten surface made for the first atom adsorption is still valid for the second beryllium atom, and the adsorption energy is even significantly larger than those of a single atom (figure 6). Very quickly (after adsorption of 10 Be atoms per cell), the adsorption energy reaches a limit (−4.0 eV, figure 6) close to the quantum calculated cohesive energy of metallic beryllium (3.7 eV) [10].

At surface completion, the adlayer (referred as the monolayer ML in the following) consists of 16 beryllium atoms regularly distributed on the tungsten surface (figure 7(a)) in four rows distant by 2.4 Å in directions parallel to the $\boldsymbol{a}$ and $\boldsymbol{b}$ crystallographic axes, this distance is imposed by the substrate and is slightly longer than in the Be bulk (2.2 and 2.3 Å according to the inter-atomic direction).

Figure 6 shows that the Be–Be interaction energy (from the energy of the adsorbed layer calculated without the substrate) provides a larger part of the cohesive energy of the system as the coverage rate of the surface increases. At coverage rates lower than 80% ML, the major part of the stabilization is brought about by the substrate–adsorbate interaction. At higher coverage, the beryllium–beryllium interaction becomes prevalent. Therefore, it is not surprising that adding an extra Be atom provokes a disordering of the adlayer structure and formation of a beryllium cluster of 7 aggregated atoms (figure 7(b)). Considering the strongly increasing effort for calculations involving further atoms, no larger systems were studied. However, considering figure 6, it can reasonably be expected that including more beryllium atoms would follow the tendency to beryllium clustering and weakened binding of these clusters to the tungsten substrate.

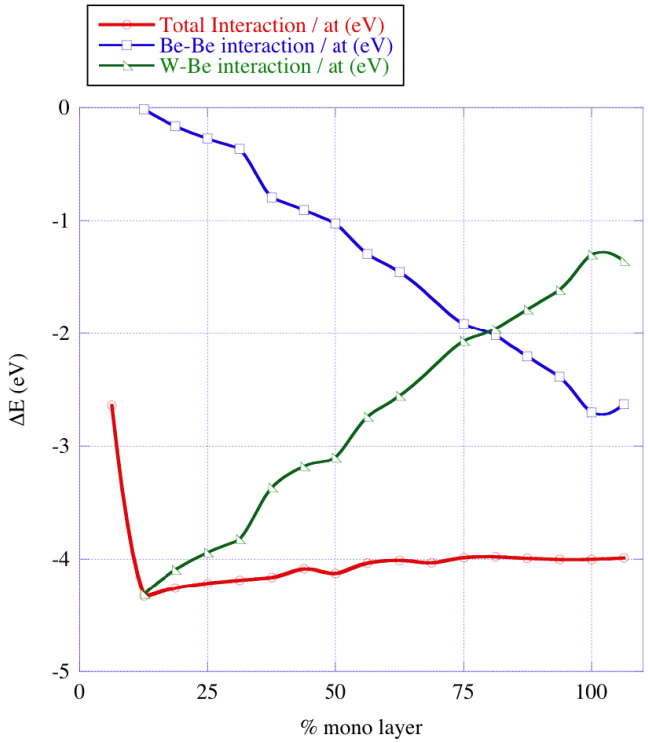


**Figure 6.** Energy profile of adsorption energies per Be atom (calculated using equation (1)) with successive atoms adsorption on W(111), the monolayer at surface completion (100%) corresponds to adsorption of 16 Be atoms per cell. The upper part curve presents the Be–Be interaction energy. The total energy is decomposed as W–Be + Be–Be interaction.

## 3. Experimental studies

The interactions between beryllium and tungsten are studied in several series of experiments. Both Be on W and the reverse system W on Be were studied by layer deposition and subsequent annealing steps. Be is deposited and sequentially annealed up to 1070 K *in situ* from the vapor phase with thicknesses up to a few nanometer on clean polycrystalline W substrates and investigated by x-ray photoelectron spectroscopy (XPS) [7, 8]. Experiments with a continuous Be influx to tungsten are performed at substrate temperatures of 1023 and 1123 K [24]. The reverse system, W on polycrystalline Be, is studied by tungsten magnetron deposition of a 200 nm layer at 300 K, sequential annealing up to 1070 K under UHV conditions, and analysis by Rutherford backscattering spectrometry (RBS) after transfer through air. After the final annealing step, a sputter depth profile with XPS analysis is performed [9]. Additional structural investigations were performed for both the Be/W and W/Be systems by x-ray diffraction (XRD) [24, 25].

Non-thermal interactions of Be as a plasma impurity were performed with polycrystalline W surfaces at elevated temperatures between 1023 and 1260 K [9, 24]. The kinetic energy of the Be particles from the plasma is ∼60 eV with an applied bias voltage of −75 V, and ∼10 eV without bias voltage. The composition of the final surface is investigated by Auger electron spectroscopy (AES), XPS, and wavelength dispersive x-ray spectroscopy (WDX).

The formation of Be–W alloys can be directly observed by XPS, e.g. in the shift of the Be 1s core level [10]. Both XPS and RBS allow a quantitative analysis of the reactions and are sensitive to different depths: XPS probes the first few nanometers, whereas RBS probes several 100 nm to a few $\mu$m, depending on the used projectile particle and primary energy. Together with sputtering of the surface by argon ions, XPS enables a depth profiling of the surface, performing a chemically resolved analysis. Using these techniques, the behavior of the Be–W system in the different experimental approaches was studied.

For the first case of thin Be layers deposited on tungsten at 300 K, a surface alloying restricted to the first monolayers is observed. Additionally deposited Be is in the metallic state. This interface alloy formation is visible in both core level shifts of the Be 1s and the W 4f lines. Also the shape of the valence band spectra changes in a characteristic way with alloy formation and exhibits a small intensity shift towards the Fermi edge [7]. Above 670 K, the alloy peak fractions increase, indicating the formation of additional alloy phase. The stoichiometry $Be_2C$ for the alloy is determined from the alloy components in the Be 1s and the W 4f intensities. At the same time, the overall Be intensity decreases with increased annealing temperature. The diffusion of Be beyond the surface alloy layer deeper into the W substrate is excluded from

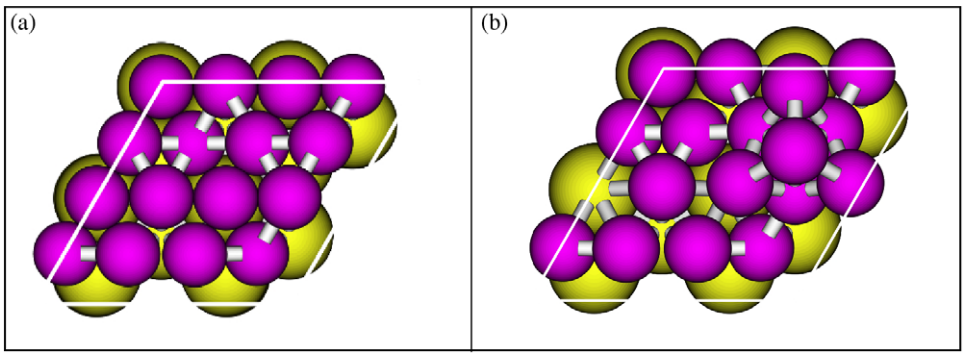


**Figure 7.** (a) Adlayer structure at W(111) surface completion (16 Be per cell). (b) An extra beryllium atom provokes the formation of Be clusters above the substrate surface.

sputter depth profiles after the annealing experiments. No Be intensity is detected beyond a depth determined by the ion-beam induced mixing. The Be sputtering depth profile is confirmed by a Monte Carlo simulation using TRIDYN. Long-term (∼3 h) annealing experiments of thin Be layers with different initial thicknesses show that, regardless of the initial Be thickness, the final alloy layer always has an equivalent Be thickness of ∼1.2 nm. Moreover, the loss of the excess Be takes place already during the temperature ramp-up. Only small additional increases in alloy amounts are observed during the annealing at constant temperature [8, 9]. From this observation, together with the sputter depth profiles, it is concluded that the $Be_2W$ alloy formation competes with Be sublimation from the surface. The $Be_2W$ alloying reaction cannot act as an efficient driving force for keeping the Be in the solid phase.

In the reverse system, W deposited on Be, the formation of a Be–W alloy starts only above 970 K, as determined from RBS spectra. However, this technique is not sensitive enough to exclude the possibility of an interface alloy formation in the order of a monolayer, as observed in the Be/W experiments. Nevertheless, the formation of a $Be_{12}W$ alloy is observed from quantitative RBS analysis. The $Be_{12}W$ alloy also exhibits characteristic core level shifts in the Be 1s and W 4f lines. The formation of a stable $Be_{12}W$ alloy layer on the Be substrate from a W layer, without a typical diffusion tail into the substrate, indicates that the system has reached an energetically favorable situation. From the temporal evolution of the alloy layer thickness a diffusion coefficient of $1.6 \times 10^{-13}$ cm$^2$ s$^{-1}$ at 1070 K is determined [9]. For 1023 and 1123 K, additional diffusion coefficients for the Be–W interdiffusion are available: $4.3 \times 10^{-15}$cm$^2$ s$^{-1}$ and $5.8 \times 10^{-13}$ cm$^2$ s$^{-1}$, respectively [24].

A third class of experiments involves Be impinging at non-thermal energies at W surfaces continuously, as a seeded impurity in a deuterium plasma. If the kinetic energy of the Be particles is high enough, sputtering of the surface must be considered. For lower Be energies (∼10 eV), the formation of Be alloys at the surface is observed for temperatures between 1070 and 1150 K [24]. At a temperature of 1260 K, Be is found in depths well above 1 $\mu$m with a concentration of 10%, although the concentration in the deuterium plasma was below 0.5%. As determined by XPS, Be is present both in the metallic and alloyed state. However, the Be 1s core level shift does not allow the decision between $Be_2W$ and $Be_{12}W$. From the experimental conditions, also the question whether the Be is transported into these depths by diffusion or whether a compound surface layer has been deposited by the plasma–surface interaction processes, cannot be decided. Nevertheless, Be is accumulated to a 10% level in the sample from a minor plasma impurity (concentration $< 0.5\%$) [9].

## 4. Discussion and conclusion

The reactivity of the two model surfaces studied here are qualitatively similar, although the W(111) surface gives rise to higher energy exchanges from and to the adsorbate, adsorption energies, as well as barriers compared to the W(100) case. However, the PES associated to W(100) and the DOS structure perturbation along reaction is easier to interpret, therefore the discussion the electronic structure is developed on this system.

From section 2, it clearly emerges that the metal surface layer relaxation leads to an electronic structure of the surface and of the two upper layers different from the electronic structure of the inner bulk (shown in [23]). The surface W(5d) peaks in the valence band are closer to the Fermi level and therefore closer to the originally empty Be(2p) energy levels in the conduction band. The orbital recombination is more efficient on the surface and yields relatively small stabilizations of −2.3 [W(100)] and −2.6 eV [W(111)] compared to the system formed by the bare W surface and the beryllium atom far from it. This stabilization is maintained along successive Be atom adsorption until formation of a complete monolayer associated to the plateau at completion. The calculations also indicate that a larger amount of beryllium on the surface should lead to a dislocation of the adlayer and formation of pure beryllium clusters.

After crossing a high energy barrier from the adsorbed state into the W bulk, the trapping of a beryllium atom into the bulk host metal does not induce a gain in total energy with respect to the separate constituents' total energy. From the energy point of view, the formation of a W–Be alloy is therefore not favored [23].

These results must be taken into consideration the approximations of the method: restricted working cell, 0 K temperature, no ZPE (zero point energy) correction. But

semi-quantitatively, they explain why the beryllium can form a monolayer film on the tungsten surface but is unable to constitute an alloy-like mixing. These DFT results can explain well the available experimental data on Be films deposited and annealed on W, summarized in section 3. The limited formation of the $Be_2W$ alloy and the competition between Be sublimation and alloy formation, together with the observation that no extended Be diffusion into the W bulk is observed, can be understood with the overall endothermic reaction, shown in figure 3. Since both W surfaces studied here by DFT show this tendency, the conclusion is valid despite the experiments being carried out on polycrystalline W substrates. The formation of a thin $Be_2W$ surface alloy layer is explained by the deep energy minima for Be adsorbed at the W surfaces. The energy required to diffuse into the W bulk is, for both W(100) and W(111), higher than the barrier for desorption (sublimation). Also the experimental shift of valence band intensity towards the Fermi edge during $Be_2W$ alloy formation is qualitatively confirmed by the DFT calculations. However, due to the different tungsten substrates in DFT calculation and experiments, not all details of the VB spectra coincide with the calculated DOS. Detailed synchrotron studies with W(100) and W(111) substrates are necessary to improve the quality of the experimental data. If Be is arriving at the surface with hyperthermic energies, as it is the case if Be is a plasma impurity, it is implanted into tungsten and the surface–subsurface barrier is of no concern. Therefore, the accumulation of a limited Be concentration in the plasma-exposed W samples can be explained.

The reverse system, i.e. adsorption of tungsten on Be(0001), was studied by DFT in earlier work [10]. Also in this case, the two metals interact through W(5d) and Be(2p) electrons. The tungsten adsorption energy, however, is markedly larger, −4.2 eV compared to −2.6 eV. In contrast to the Be adsorption on W, tungsten trapping into beryllium yields a total energy gain of 4.8 eV compared to the non-interacting system. In view of these DFT results, the formation of the limited and stable $Be_{12}W$ alloy layer, observed in the annealing experiments of W films on Be, is explained. Diffusion of W into the Be bulk would require the dissolution of the energetically favorable alloy stoichiometry. However, also in the case of W on Be, a surface–subsurface barrier exists and alloying is experimentally only observed above 970 K.

The most important result for the tokamak first wall cladding is that beryllium inclusion into tungsten is energetically unfavorable (endothermic), whereas tungsten in beryllium is more stable than the non-interacting system (exothermic situation). Therefore, thermally, even if the temperature is high enough to surmount the barrier for beryllium subsurface diffusion, the resulting compound will not be stable. The energetic stability of Be adsorbed on W(100) implies, within the limits of the approximations of this calculation, that a film of beryllium can be synthesized on W(100), but the adatoms can hardly mix with the substrate to form an alloy.

Nevertheless, beryllium inclusion into the host metal can result from plasma conditions, when tungsten cladding is bombarded by energetic beryllium impurities originating from the boundary plasma. It was shown that the alloy structure produced by W bombardment of Be(0001) is quite similar to the structure of the already known $Be_{12}W$ alloy [10]. In this compound, the Be–W bond length can be 2.55 or 2.77 Å.

In summary, concerning the studied tungsten surfaces reactivity toward beryllium, quantum and spectroscopic studies point to the convergent conclusions that:

(i) Alloy is formed at the interface of both W/Be and Be/W systems, but only a very thin film of beryllium on the tungsten surface. This is consistent with the quantum result on the non-stability of Be inclusion in W bulk.
(ii) In case of alloy formation by a high energy Be atom impinging of the W surface, its structure is different from the alloy formed in the reverse system, and this is also consistent with the quantum result. From a quantum point of view, the Be–W bond lengths are different in the two systems.

The next step should be to investigate the reactivity of this film toward hydrogen isotopes given the very important reactivity of beryllium towards oxygen.

## Acknowledgments

This work, supported by the European Communities under the contract of Association between EURATOM, CEA and the French Research Federation for fusion studies, was carried out within the framework of the European Fusion Development Agreement. The views and opinions expressed herein do not necessarily reflect those of the European Commission. It is also supported by the 'Agence Nationale de la Recherche' (ANR CAMITER No. ANR-06-BLAN-0008-01). The calculations were performed at the CEA computing Center (CCRT).

## References

[1] Wesson J 2004 *Tokamaks* (Oxford: Oxford Science Publications)
[2] ITER website http://www.iter.org/
[3] Doerner R P 2007 *J. Nucl. Mater.* **363–365** 32
[4] Doerner R P, Baldwin M J and Causey R A 2005 *J. Nucl. Mater.* **342** 63
[5] Doerner R P, Baldwin M, Hanna J, Linsmeier Ch, Nishijima D, Pugno R, Roth J, Schmid K and Wiltner A 2007 *Phys. Scr.* T **128** 115
[6] Linsmeier Ch, Luthin J and Goldstraß P 1999 *J. Nucl. Mater.* **290–293** 25
[7] Wiltner A and Linsmeier Ch 2006 *New J. Phys.* **8** 181
[8] Wiltner A and Linsmeier Ch 2005 *J. Nucl. Mater.* **337–339** 951
[9] Linsmeier Ch, Ertl K, Roth J, Wiltner A, Schmid K, Kost F, Bhattacharyya S R, Baldwin M and Doerner R P 2007 *J. Nucl. Mater.* **363–365** 1129
[10] Allouche A and Linsmeier Ch 2008 *J. Phys.: Conf. Ser.* **117** 012002
[11] Huang S F, Chang R S, Leung T C and Chan C T 2005 *Phys. Rev.* B **72** 75433
[12] http://www.quantum-espresso.org and http://www.pwscf.org
[13] Kwak K W, Chou M Y and Troulllier N 1996 *Phys. Rev.* B **53** 13734
[14] Holzwarth N A W, Chervenak J A, Kimmer C J, Zeng Y, Wu W and Adams J 1993 *Phys. Rev.* B **48** 12136
[15] Allouche A 2008 *Phys. Rev.* B **78** 085429

[16] Pallassana V, Neurock M, Hansen L B, Hammer B and Nørskov J K 1999 *Phys. Rev.* B **60** 6146 and references therein
[17] Hammer B, Morikawa Y and Nørskov J K 1996 *Phys. Rev. Lett.* **76** 2141
[18] Szabo A and Ostlund N S 1982 *Modern Quantum Chemistry* (New York: McGraw-Hill)
[19] Posternak M, Krakauer H, Freeman A J and Koelling D D 1980 *Phys. Rev.* B **21** 5601
[20] Posternak M, Krakauer H and Freeman A J 1982 *Phys. Rev.* B **25** 755
[21] Wimmer E, Freeman A J, Hiskes J R and Karo A M 1983 *Phys. Rev.* B **28** 3074
[22] Chen L, Sholl D S and Johnson J K 2006 *J. Phys. Chem.* B **110** 1344
[23] Allouche A 2009 *Chem. Phys. Lett.* **470** 119
[24] Baldwin M J, Doerner R P, Nishijima D, Buchenauer D, Clift W M, Causey R A and Schmid K 2007 *J. Nucl. Mater.* **363–365** 1179
[25] Wiltner A, Kost F, Lindig S and Linsmeier Ch 2007 *Phys. Scr.* T **128** 133